Studies on the photoluminescence and thermoluminescence properties of $CaZrO_3$:xEu^{3+} phosphor for dosimetric application

Marjaneh Jafari Fesharaki,[1,*] Mohammad Reza Jalali,[1] Leila Karimi,[1] and Ehsan Sadeghi[2,3]

[1]*Department of Physics, Payame Noor University, P. O. Box 19395-3697, Tehran, Iran*

[2]*TL Laboratory, Physics Deparment, University of Kashan, Kashan, Iran*

[3]*Institute of Nanoscience and Nanotechnology, University of kashan, Kashan, Iran*

(Dated: September 13, 2021)

Abstract

Series of $CaZrO_3$:xEu^{3+} (x=0.01, 0.02, 0.03, 0.04 and 0.05) phosphors have been prepared by low temperature sol-gel auto combustion method. The structure and morphology of the samples were investigated by X-ray diffraction (XRD) and field-emission scanning electron microscope (FE-SEM). The energy-dispersive X-ray spectroscope (EDX) was employed to analyze the elemental composition of the phosphor. The XRD patterns indicated that the sample was single phase at 350 °C with a perovskite structure. The optimum temperature for the single- phase and crystalline phosphors of $CaZrO_3$:xEu^{3+} was 700 °C. Study of photoluminescence (PL) at room temperature showed that the phosphors can be excited by light with a wavelength of 391 nm. The results of emission spectrum showed that the red luminescence of $CaZrO_3$:xEu^{3+} due to electric dipole transition of $^5D_0 \rightarrow {}^7F_2$ was dominant at wavelength of 615 nm and weaker transition at wavelength of 590 nm which was due to magnetic dipole transition of $^5D_0 \rightarrow {}^7F_1$. For the thermoluminescence (TL) study the prepared sample irradiated by X-ray lamp, the TL curve was then recorded at fixed heating rate of 2 °C/s. The TL glow curve showed well single peak at a temperature of 165 °C. The effect of Eu^{3+} concentration at fixed X-ray exposure time was studied and maximum TL occurred at x=0.02. Also the variation of TL intensity with X-ray time (5 to 15 min) showed linear response with dose. The TL glow peak shows more stability and less fading in prepared phosphor which is suitable for TL dosimetry.

* m.jafari.fesharaki@pnu.ac.ir

I. INTRODUCTION

The main group of compounds are oxides with ABO_3 formula with perovskite structure. Solar cell, energy harvesting device, solid electrolyte, anode material in solid oxide fuel cell, photocatalyste, sensors, fillers, satellite broadcasting, crystalline host for phosphor materials and multilayer capacitors are some applications of these oxides [1–5]. One of the most common perovskite compounds is calcium zirconate ($CaZrO_3$) with a high melting point (2600 °C) and band gap of 5.6 eV which can be used as host phosphor [6–8].

Rare earth (RE) ions such as Eu, Tm, Ce, Sm, Gd, Er and Pr can be doped in $CaZrO_3$ host and improve the luminescence properties [9]. A luminescence material commonly emits in the visible region of the electromagnetic spectrum but they can also emit in the ultraviolet (UV) and infrared (IR) regions depending upon the activator ion doped [8]. $CaZrO_3$:Tm showed blue emission [10]; $CaZrO_3$:Pr showed green emission [11], $CaZrO_3$:Ce displayed violet and blue emission [12]; $CaZrO_3$:Sm,Gd indicated yellow-orange emission [13]; $CaZrO_3$:Er and $CaZrO_3$:Er, Ce revealed green photoluminescence emission [14]. Europium ion is popular as an activator dopant for many different in organic lattices producing red light emission [2].

The use of thermoluminescence for dosimetry in medical, personal and environmental fields is now very popular. Among the most important properties that can be considered for an ideal dosimetry are: low sensitivity and fading, high stability, linear dosimetry in a dose range and having the ability to use repeatedly without any changing in the sensitivity of the luminescence properties [15–17].

In recent years, the use of nanomaterials in various fields has grown a lot. As the particle size decreases, the surface to volume ratio of these materials increases. This makes various properties such as optical and dosimetric of nanomaterials to their mass state, and this is because they have a high ability to create trapping with high surface centers. Today, several methods are used to produce powders with nanometer dimensions. These methods are: solid state [18], precipitation [19], hydrothermal [20] and sol-gel method [9, 21]. In this study, $CaZrO_3$:xEu^{3+} phosphors were produced by sol-gel auto combustion method in low temperature and the optical properties were investigated. The thermoluminescence glow curve under X-ray exposure was performed for the first time.

II. EXPERIMENTAL DETAILS

The starting materials are high purity $Ca(NO_3)_2.4H_2O$, ZrN_2O_7, $Eu(NO_3)_3.6H_2O$ and $C_6H_8O_7.H_2O$ (citric acid) as fuel. $Ca_{1-x}ZrO_3$:xEu^{3+} is synthesized by auto combustion sol-gel method and the chemical equation for the reaction is:

(1-x)$Ca(NO_3)_2.4H_2O$+x$Eu(NO_3)_3.6H_2O$+ZrN_2O_7+ 1.2$C_6H_8O_7 \longrightarrow Ca_{1-x}ZrO_3$:$xEu^{3+}$ (s)+gaseous products

According to nominal composition of $Ca_{1-x}ZrO_3$:xEu^{3+} (x=0.01, 0.02, 0.03, 0.04 and 0.05), a stoichiometric amount of metal nitrates were dissolved separately in minimum quantity of deionized water, then citric acid was added in this solution with molar ratio of citric acid to nitrates based on total oxidizing and reducing valencies of oxidizer and fuel (citric acid) according to concept used in propellant chemistry [22]. During the heating, pH of the solution was set to 7 [23] using ammonia solution and the solution was placed on a magnetic stirrer for 20 min at 80 °C until a resin solution was obtained, then transfered into a preheated furnace maintained at 350 °C. The material underwent rapid dehydration and foaming followed by decomposition, generating combustible gases. Finally the soft gray powder was obtained. In order to form the final phases and clear the existing carbons, the powder will be placed in the electric furnace at various temperature ranging from 550 to 1000 °C for 3 h to increase the brightness. An X-ray diffractometer (Philips Expert) was employed using a Cu-Kα (λ=1.5406 Å) radiation in the range of 2θ=20-80° as a source for characterizing the samples. Then the microstructure of samples was analyzed using a field emission scanning electron microscopy (FE-SEM; modelS-4160). Also, the compositions were examined by energy-dispersive X-ray spectroscopy (EDX) in the scanning electron microscope (SEM). Photoluminescence (PL) spectrum was recorded using a Perkin-Elmer spectrometer model LS55 with photo multiplier tube and Xenon lamp at room temperature. Finally, the thermoluminescence (TL) response was recorded by a Harshaw model 4500 computer based TL reader. A heating rate of 2 °C/s was used for recording glow curves.

III. RESULTS AND DISCUSSION

The structure and phase purity of the powders can be examined by XRD. The XRD patterns of $CaZrO_3$ powders calcined at various temperatures before and after annealing at different temperatures ranging from 550 to 1000 °C are shown in Fig. 1 (a). Below 550 °C, the diffract patterns

TABLE I. Structural analysis with particle size by XRD technique for $Ca_{0.98}Eu_{0.02}ZrO_3$ phosphor.

S. No.	h k l	2θ	$FWHM$	$D(nm)$
1	(101)	22.15	0.28	28
2	(121)	31.55	0.34	24
3	(202)	45.25	0.33	26
4	(042)	55.65	0.69	13
5	(123)	56.7	0.62	15
6	(004)	65.85	0.48	19
7	(203)	74.8	0.65	17

show weak crystalline structure of perovskite, which can be matched to orthorhombic $CaZrO_3$ phase (JCPDS No. 35-0790). By increasing the temperature up to 550 °C, the additional phases gradually diminish. The diffraction peaks considerably intensify at calcination temperatures above 700 °C, indicating improvement of the structure with an annealing process. To study the effect of europium doping on the structural parameters (with the space group of Pbnm) of the perovskite $CaZrO_3$ powder, variable concentration of Eu (0.01-0.05) was added and a same calcination was conducted. The corresponding XRD patterns are shown in Fig. 1 (b). Since the radius of Eu^{3+} ion (0.095 nm) and Ca^{2+} ion (0.099 nm) are close to each other, europium is expected to substitute calcium, not zirconium with radius of 0.072 nm [24]. XRD patterns in Fig.1 (b) show no considerable variation due to doping, indicating the negligible effect in the used Eu range on the lattice parameters.

The size of the $Ca_{0.98}Eu_{0.02}ZrO_3$ crystallite was calculated using the Debye Sherer formula [25]:

$$D = 0.9\frac{\lambda}{\beta cos\theta} \tag{1}$$

where D is particle size, β is FWHM (full width half maximum), λ is the wavelength of X-ray source (0.154 nm) and θ is the angle of diffraction. The structural information and particle size calculation is present in Table I, which shows the crystallite size across the most intense peak i.e.(121) direction is 24 nm.

FE-SEM and EDX pictures are shown in Fig. 2 and Fig. 3, respectively. Fig. 2 (a) and (b) reveal agglomerates with 130 nm and 123 nm average size that are constructed from small particles with spherical and polyhedron shapes. The EDX spectrum of $CaZrO_3$ in Fig. 3 (a) indicates the presence of barium, zirconium, oxygen elements with concentration as shown inside. In Fig. 3

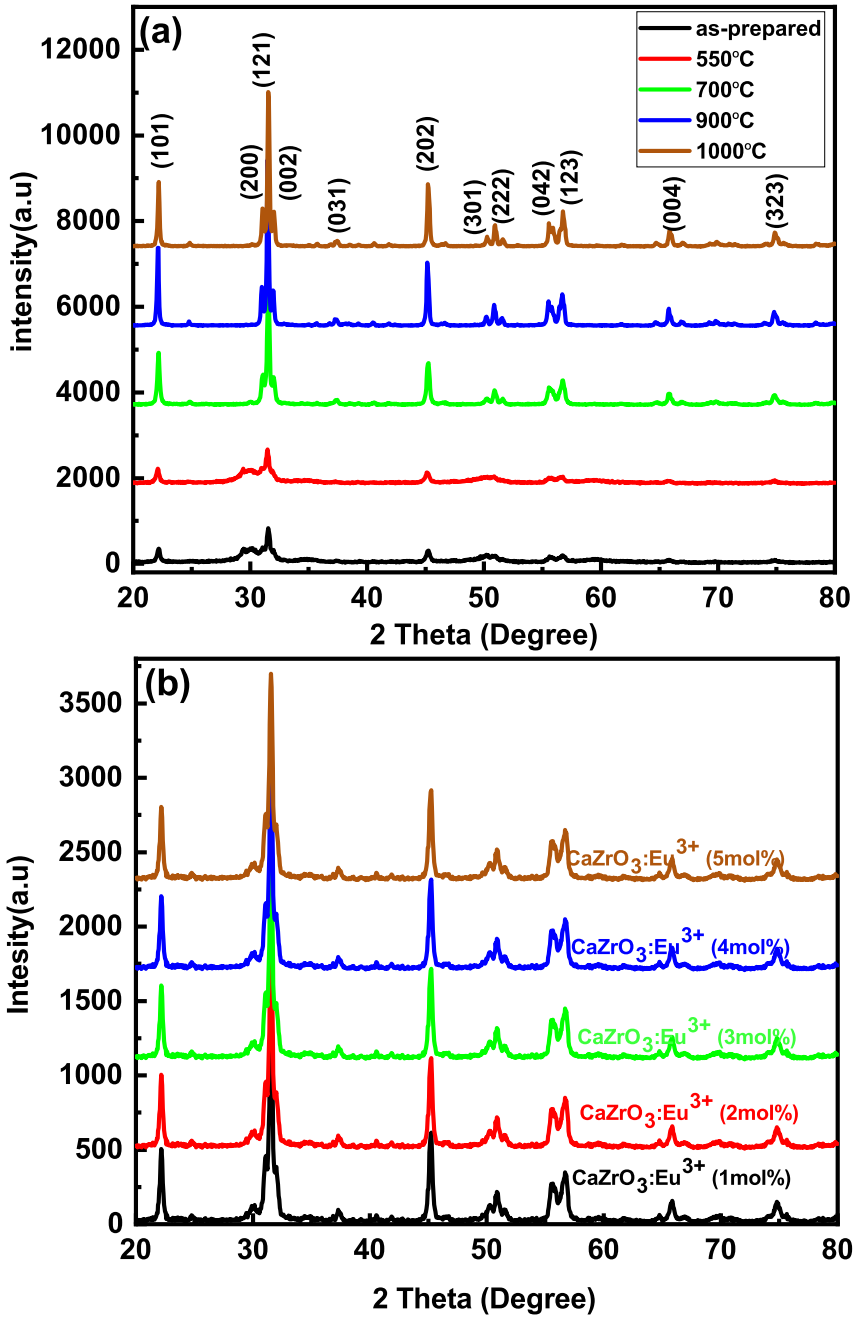

FIG. 1. XRD pattern of (a) $CaZrO_3$ powders calcined at various temperatures and (b) $Ca_{1-x}ZrO_3$:xEu^{3+} (0.01-0.05) doped phosphor.

(b), in addition to the elements mentioned, eurobium is also visible.

The PL excitation spectrum of $Ca_{0.98}Eu_{0.02}ZrO_3$ calcined at 700 °C is shown in Fig. 4. The spectrum includes two parts; (1) broad band region (200 nm-300 nm) peaking at 268 nm is called charge transfer (CT) state band that can be attributed to CT transition from 2p orbital of O^{2-} ions to an empty 4f orbital of Eu^{3+} ions ($O^{2-} \rightarrow Eu^{3+}$)[18], (2) several sharp lines in the range

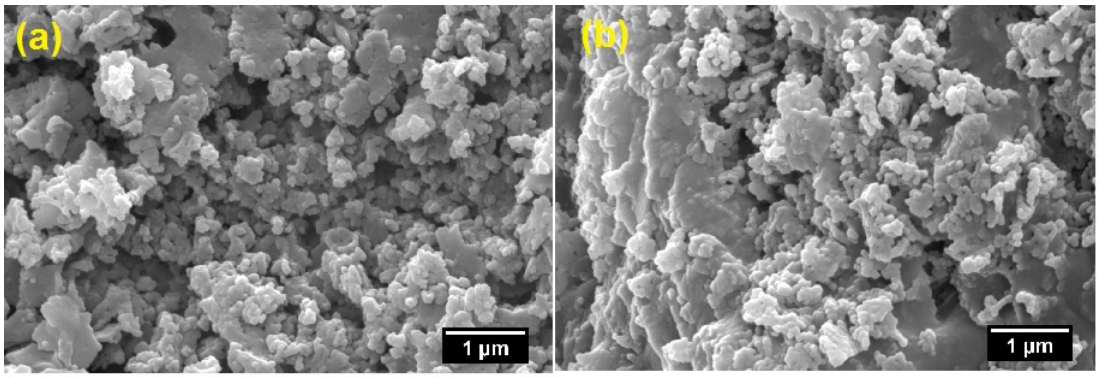

FIG. 2. FE-SEM images of (a) $CaZrO_3$ and (b) $Ca_{0.98}Eu_{0.02}ZrO_3$ phosphor, calcined at 700 °C for 3 h.

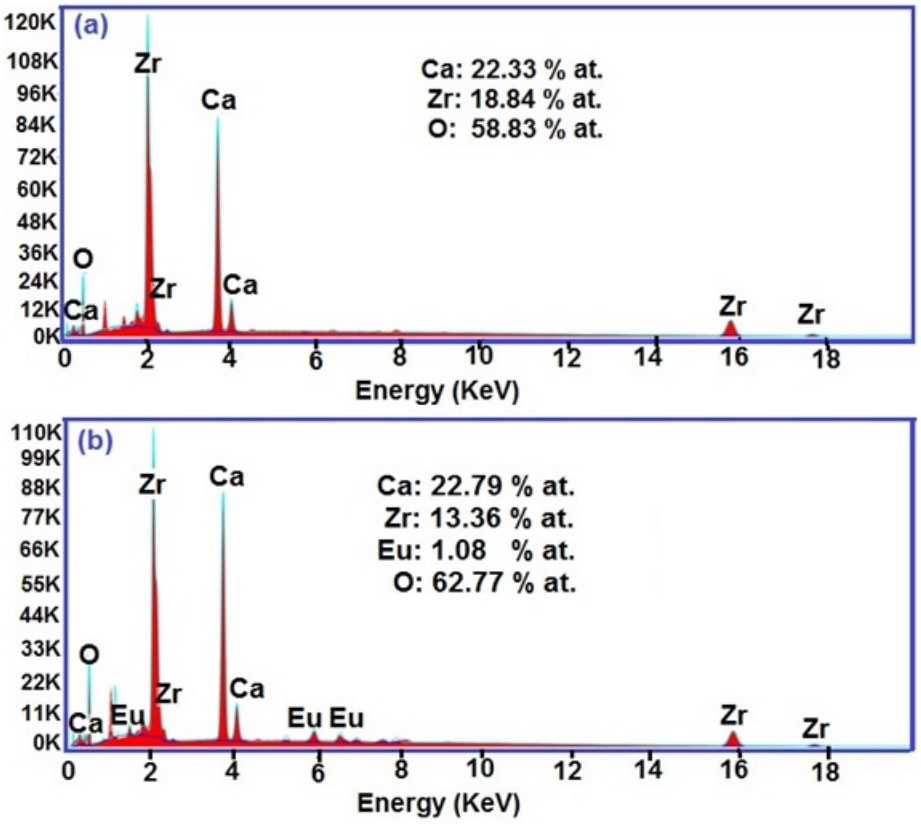

FIG. 3. The EDX images of (a) $CaZrO_3$ phosphor calcined at 700 °C for 3 h, (b) $Ca_{0.98}Eu_{0.02}ZrO_3$ phosphor calcined at 700 °C for 3 h.

of 320 to 500 nm are related to the configurational 4f-4f transition of Eu^{3+} in host lattices. The strongest sharp peak located at 391 nm corresponds to $^7F_0 \rightarrow {}^5L_6$ transition of Eu^{3+} ions. The weak peaks can be attributed to transitions of $^7F_0 \rightarrow {}^5D_4$,$^7F_0 \rightarrow {}^5G_J$,$^7F_0 \rightarrow {}^5L_7$, $^7F_0 \rightarrow {}^5D_3$ and $^7F_0 \rightarrow {}^5D_2$ at wavelengths of 353, 368, 376, 411 and 465 nm, respectively [26]. The shape and position of

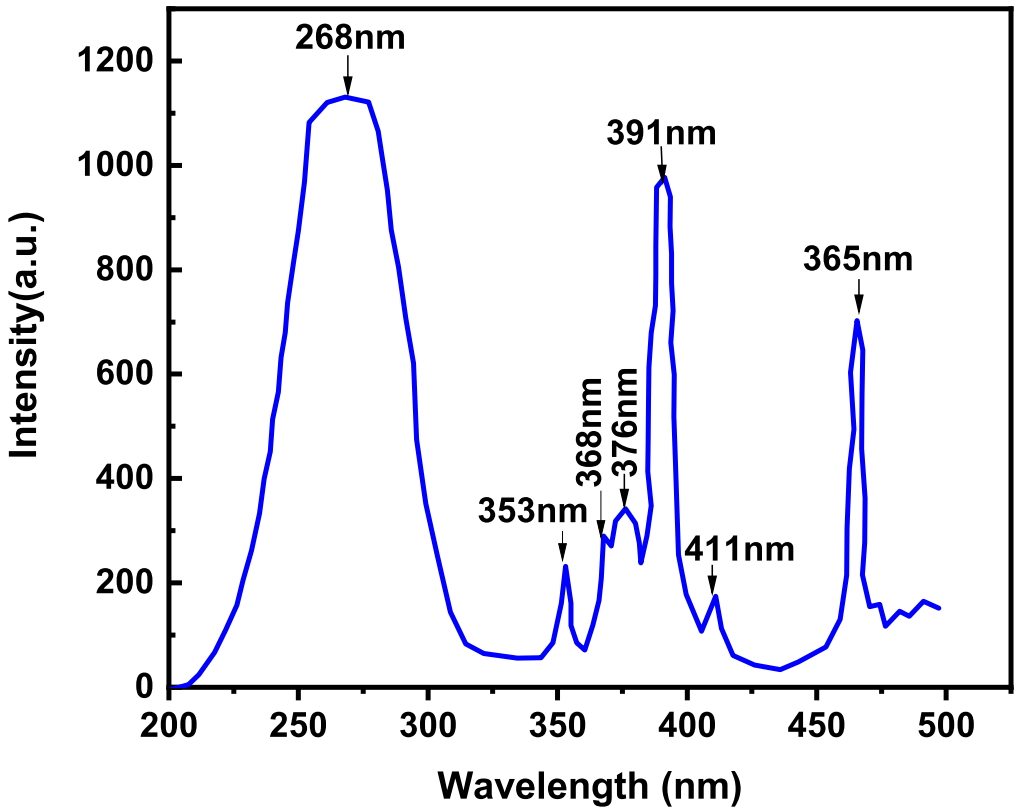

FIG. 4. PL excitation spectrum of $Ca_{0.98}Eu_{0.02}ZrO_3$ phosphor.

the photoluminescence spectrum do not change by different excitation wavelengths and only the intensity of emission spectrum changes [27]. The PL emission spectrum of $Ca_{1-x}ZrO_3$:xEu^{3+} (x=0.01, 0.02, 0.03, 0.04 and 0.05) under excitation wavelength of 391 nm are shown in Fig. 5. This spectrum of phosphor consist of peaks due to 4f configuration of Eu^{3+} transitions $^5D_0 \rightarrow {}^7F_J$ (J=0-4) at wavelengths of 578, 590, 615, 651 and 697 nm, respectively.

The orange emission at wavelengths of 590 nm belonging to $^5D_0 \rightarrow {}^7F_1$ magnetic dipole transition which is insensitive to site symmetry of Eu^{3+} ions, and the transition varies with the crystal field strength. The red emission at wavelengths of 615 nm ascribes to the $^5D_0 \rightarrow {}^7F_2$ electric dipole transition which is sensitive to local symmetry of Eu^{3+} and depends on the symmetry of the crystal field [18]. PL intensity of $Ca_{1-x}ZrO_3$:xEu^{3+} (x=0.01-0.05) increases with increasing Eu^{3+} concentration, reaching a maximum value at x=0.02 and thereafter decreases with further increase in impurity concentration. The maximum Eu^{3+} concentration in $CaZrO_3$:xEu^{3+} led to the quenching of luminescence due to energy non-radiative transition induced by the cross relaxation between adjacent Eu^{3+} ions [14] . As the Eu^{3+} concentration increases, no change in the shape and position

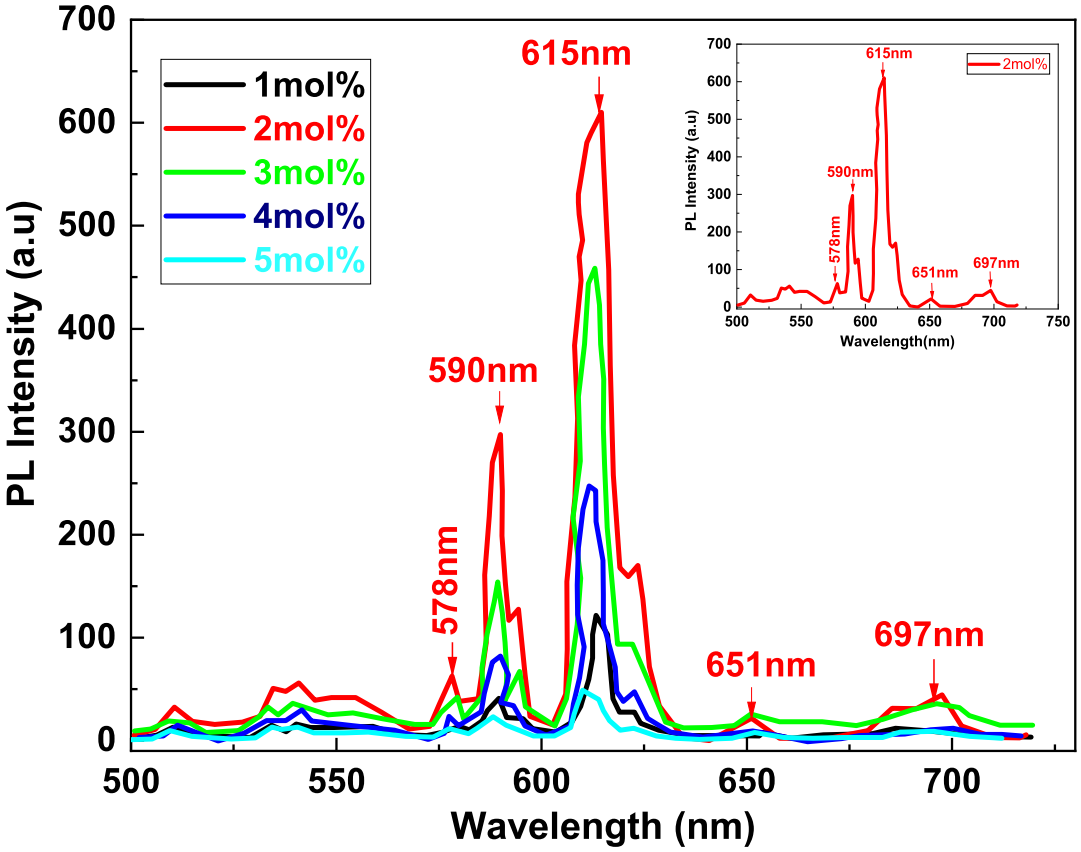

FIG. 5. PL emission spectra of $Ca_{1-x}ZrO_3$:xEu^{3+} (0.01-0.05).

intensity of PL peaks is observed (Fig. 5).

Figure 6 shows the thermoluminescence curve for samples $CaZrO_3$:xEu^{3+} (x=0.01-0.05) at heating rate of 2 °C/s. The sensitivity of thermoluminescence materials strongly depends on the type and concentration of impurities added to the host material. To find the optimal thermoluminescence radiation in terms of impurity concentration, the X-ray radiation dose is kept constant while the Eu concentration is changed. According to the Fig. 6 the shape of the curve for all concentration does not change and the TL curve for $Ca_{0.98}Eu_{0.02}ZrO_3$ displays a single radiative peak at 164 °C with highest intensity.

Essential properties of good thermoluminescence dosimeter is the stability and repeatability. To investigate the fading of $Ca_{1-x}ZrO_3$:xEu^{3+}, irradiated phosphors before reading kept in a dark room for 20 days. Fig. 7 (a) shows that the fading is negligible and this sample is stable. In order to investigate the repeatability, the sample is first annealed at 500 °C for one hour, then irradiated, and finally read. This process was repeated five times. As shown in Fig. 7 (b), the sensitivity of the sample has changed by approximately less than 4% compared to the initial state. During this

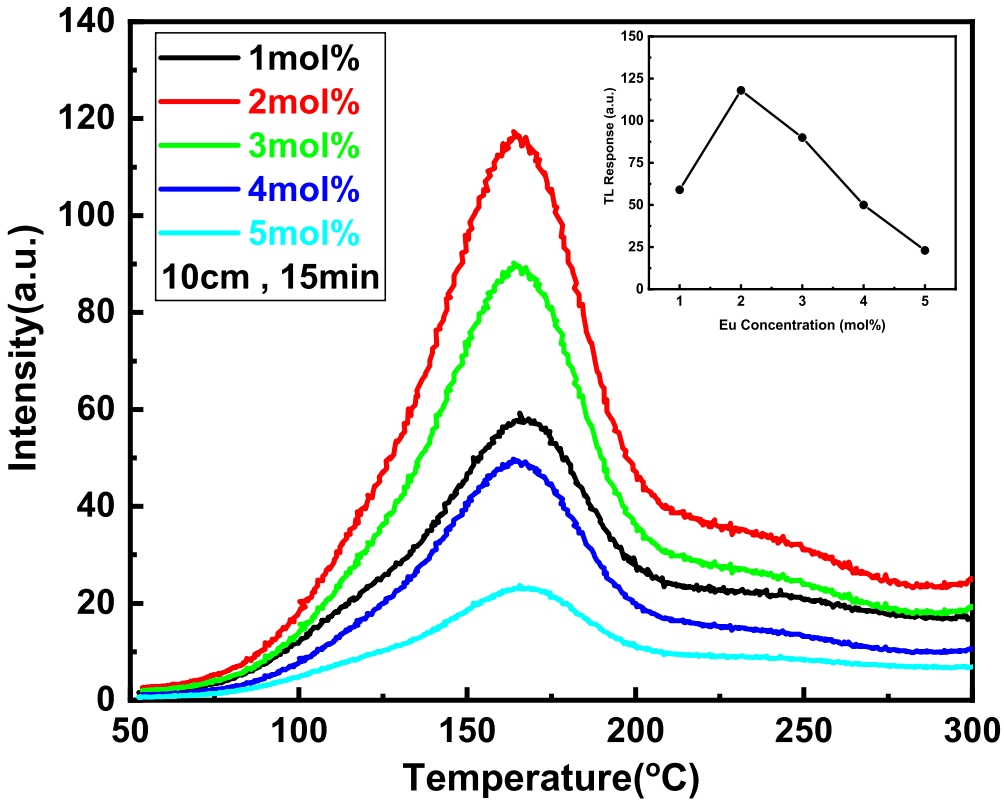

FIG. 6. TL glow curve of $Ca_{1-x}ZrO_3$:xEu^{3+} (0.01-0.05) with the constant of X-ray time.

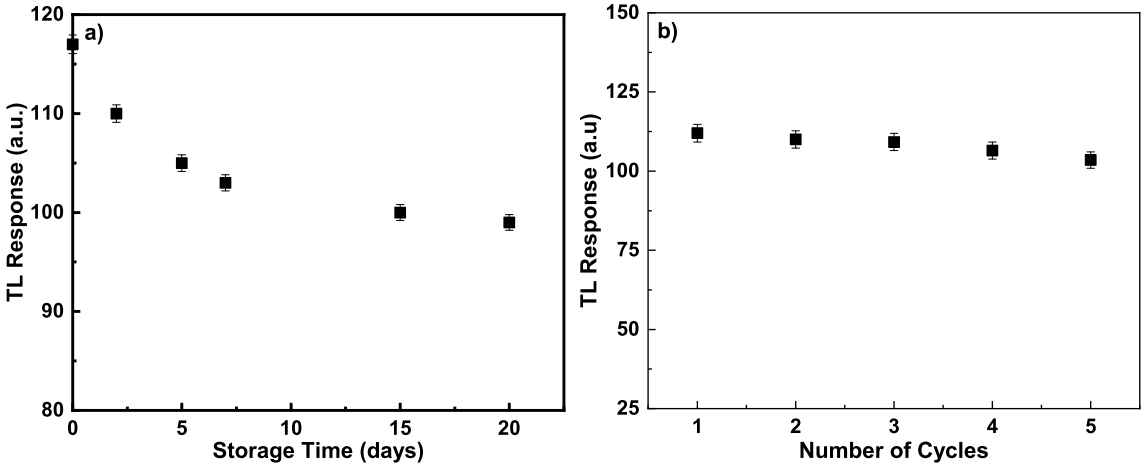

FIG. 7. (a) TL response of the $Ca_{0.98}Eu_{0.02}ZrO_3$ phosphor against the storage time at room temperature for X-ray exposer. (b) The stability of the TL response of $Ca_{0.98}Eu_{0.02}ZrO_3$ phosphor for 5 cycles for X-ray exposer.

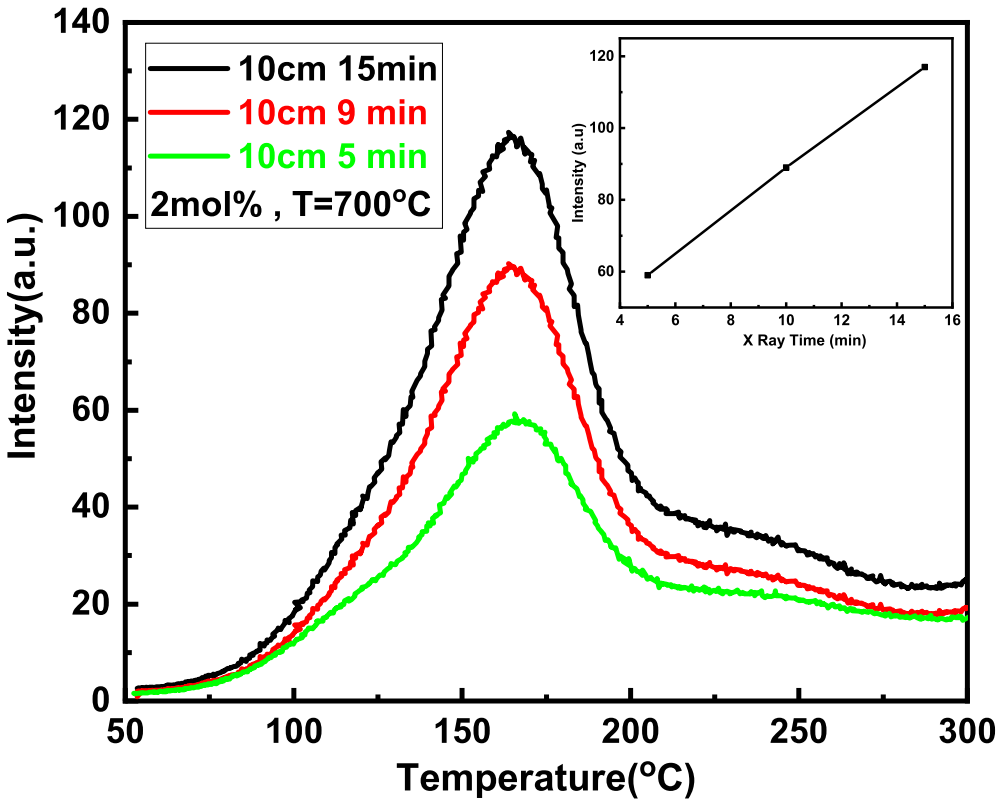

FIG. 8. TL glow curve of $Ca_{0.98}Eu_{0.02}ZrO_3$ phosphor with the variation of X-ray time.

study, glow curve of the $Ca_{0.98}Eu_{0.02}ZrO_3$ sample was investigated for different X-ray irradiation times for 5, 9 and 15 minutes (Fig. 8). The TL intensity increases with the X-ray time exposer and has linear response (at the inset).

Given that thermoluminescence curves are a suitable tool for obtaining information about trapping parameters and full description of the thermoluminescence characteristics of a TL material; it is very necessary to calculate the trapping parameters. The Tl glow curves can be analyzed in a variety of methods, among which the peak shape method is the most common method for calculating the various kinetics parameters [i.e. activation energy (E), order of kinetics (b) and frequency factor (s)]. TL parameters of prepared phosphors were calculated by peak shape method with the variation of X-ray exposures. The relationship between the frequency factor, (s) and the activation energy , (E) is given by equation (2) [18, 28].

$$s = \frac{\beta E}{K T_m^2} . \frac{1}{1 + (b-1)\,\Delta_m} . exp \frac{E}{K T_m} \tag{2}$$

where K is Boltzmann constant, b is order of kinetics, T_m is maximum temperature and β is

heating rate (=2 °C/s) in this work. The fallowing kinetic parameters calculated using peak shape method [29].

$$\sigma = T_2 - T_M, \tau = T_M - T_1, \omega = T_2 - T_1, \mu = \sigma/\omega = (T_2 - T_M)/(T_2 - T_1) \tag{3}$$

The general expression for activation energy or trap depth (E) that is obeyed for all orders of kinetics proposed by Chen [30].

$$E_\eta = C_\eta \frac{KT_m^2}{\eta} - b_\eta(2KT_m) \tag{4}$$

where, η stands for τ, σ and ω, respectively. C_η and b_η are obtained using the expressions given by equation 5 and 6, respectively [31].

$$C_\tau = 1.51 + 3(\mu - 0.42), C_\sigma = 0.976 + 7.3(\mu - 0.42), C_\omega = 2.52 + 4.2(\mu - 0.42), \tag{5}$$

$$b_\tau = 1.58 + 4.2(\mu - 0.42), b_\sigma = 0, b_\omega = 1 \tag{6}$$

Chen formula provides a method that identify the kinetics order of one trap according to the shape of the TL band. μ is the shape factor and the difference between first and second order TL glow peak. μ=(0.39-0.42) for the first order kinetics, (0.42-0.48) for the mixed order kinetics and (0.49-0.52) for the second order kinetics, respectively [32]. The TL emission intensity is recorded maximum for $Ca_{0.98}Eu_{0.02}ZrO_3$ phosphor. The TL kinetic parameters for the $Ca_{0.98}Eu_{0.02}ZrO_3$ phosphor was calculated by the peak shape method (Table II). The value of μ varying from 0.45 to 0.48 show mixed order kinetics. The required energy for escaping one electron from trap center known as activation energy or trap depth (E) calculated by Chen formula presented in Table III. The low value of activation energy (from 0.50 to 0.69 eV) confirms the trapping of electrons in shallow trapping sites [33].

IV. CONCLUSION

In this study, $CaZrO_3$:xEu^{3+} (x=0.01-0.05) phosphors synthesized by sol-gel auto combustion method were subjected to structural and optical studies.The structural study confirmed phase purity and homogeneity of the samples. The FE-SEM pictures indicated the spherically shaped particles

TABLE II. Calculation of kinetic parameters; shape factor (μ), activation energy (E) and frequency factor (s) for $Ca_{0.98}Eu_{0.02}ZrO_3$ phosphor for different X-ray irradiation time.

X-ray time	$T_1(^\circ C)$	$T_m(^\circ C)$	$T_2(^\circ C)$	τ	δ	ω	μ	$E(eV)$	s
5 min	132.2	165.6	197.1	33.4	31.5	64.9	0.48	0.8	$3.3 * 10^{10}$
9 min	133.3	163.8	191.5	30.5	27.7	58.2	0.48	0.91	$6.0 * 10^{11}$
10 min	132	164	190	32	26	58	0.45	0.91	$6.2 * 10^{11}$

TABLE III. The trap depth for the prominent glow peaks of the studied $Ca_{0.98}Eu_{0.02}ZrO_3$ phosphor evaluated from mixed order kinetics.

Chen formula	5 min X-ray	9 min X-ray	15 min X-ray
$E_\tau = c_\tau \frac{kT_m^2}{\tau} - b_\tau(2kT_m)$	0.63 (eV)	0.69 (eV)	0.66 (eV)
$E_\sigma = c_\delta \frac{kT_m^2}{\delta} - b_\delta(2kT_m)$	0.50 (eV)	0.58 (eV)	0.62 (eV)
$E_\omega = c_\omega \frac{kT_m^2}{\omega} - b_\omega(2kT_m)$	0.57 (eV)	0.56 (eV)	0.64 (eV)

with various dimensions. The phosphors excited at wavelength of 391 nm and exhibited orange-red emission with dominate peaks at wavelength of 590 and 615 nm due to the magnetic dipole $^5D_0 \rightarrow {}^7F_1$ and electric dipole $^5D_0 \rightarrow {}^7F_2$ transition of Eu^{3+} ions, respectively. The maximum TL intensity is obtained for phosphor of $Ca_{0.98}Eu_{0.02}ZrO_3$ ($2mol\%$), which has a single peak at maximum temperature of 165 °C and showed a linear response with X-ray radiation exposure time. The TL kinetic parameter for this sample showed the mixed order kinetics with low activation energy.

REFERENCES

[1] M. Noh and Y. Lee, Journal of nanoscience and nanotechnology **15**, 8267 (2015).

[2] A. K. Kunti, N. Patra, R. A. Harris, S. K. Sharma, D. Bhattacharyya, S. N. Jha, and H. C. Swart, Inorganic Chemistry Frontiers **8**, 821 (2021).

[3] H. Tang and X. Zhang, in *IOP Conference Series: Earth and Environmental Science*, Vol. 639 (IOP Publishing, 2021) p. 012025.

[4] H. Fukushima, D. Nakauchi, T. Kato, N. Kawaguchi, and T. Yanagida, Journal of Luminescence **223**, 117231 (2020).

[5] S. Tripathi, R. Tiwari, A. Shrivastava, V. K. Singh, N. Dubey, and V. Dubey, Optik **157**, 365 (2018).

[6] P. Stoch, J. Szczerba, J. Lis, D. Madej, and Z. Pdzich, Journal of the European Ceramic Society **32**, 665 (2012).

[7] R. Ianoş and P. Barvinschi, Journal of solid state chemistry **183**, 491 (2010).

[8] S. K. Gupta, P. Ghosh, N. Pathak, and R. Tewari, RSC Advances **5**, 56526 (2015).

[9] H. Zhang, X. Fu, S. Niu, and Q. Xin, Journal of alloys and compounds **459**, 103 (2008).

[10] H. Zhang, X. Fu, S. Niu, and Q. Xin, Journal of luminescence **128**, 1348 (2008).

[11] E. Pinel, P. Boutinaud, and R. Mahiou, Journal of Alloys and Compounds **380**, 225 (2004).

[12] B. Evangeline, P. A. Azeem, R. P. Rao, G. Swati, and D. Haranath, Journal of Alloys and Compounds **705**, 618 (2017).

[13] D. Qingqing, Z. Guangjun, Z. Juan, Z. Haifeng, Z. Jie, and Y. Zhongsen, Journal of Rare Earths **30**, 1000 (2012).

[14] Q. Du, G. Zhou, J. Zhou, H. Zhou, and J. Zhan, Materials Research Bulletin **47**, 3774 (2012).

[15] M. Zahedifar and E. Sadeghi, Radiation protection dosimetry **157**, 303 (2013).

[16] N. Salah, N. D. Alharbi, S. S. Habib, and S. Lochab, Journal of Luminescence **167**, 59 (2015).

[17] M. Zahedifar, F. Almasifard, E. Sadeghi, S. Harooni, and M. K. Biroon, Radiation Measurements **103**, 26 (2017).

[18] I. P. Sahu, D. Bisen, R. K. Tamrakar, K. Murthy, and M. Mohapatra, Journal of Science: Advanced Materials and Devices **2**, 69 (2017).

[19] X. Han, L. Zhao, J. Zhang, Q. Jin, R. Xu, B. Cui, X. Lei, *et al.*, Journal of Materials Science: Materials in Electronics **31**, 13088 (2020).

[20] S. D. Meetei and S. D. Singh, Journal of alloys and compounds **587**, 143 (2014).

[21] Q. Fan, D. Li, J. Li, and C. Wang, Journal of Alloys and Compounds **829**, 154483 (2020).

[22] V. Taxak, R. Arora, S. Khatkar, *et al.*, Journal of rare earths **32**, 293 (2014).

[23] B. Evangeline and P. A. Azeem, Materials Today: Proceedings **3**, 3901 (2016).

[24] J. Huang, L. Zhou, Y. Lan, F. Gong, Q. Li, and J. Sun, Central European Journal of Physics **9**, 975 (2011).

[25] N. Tiwari, R. Kuraria, and S. Kuraria, Optik **126**, 3488 (2015).

[26] D. Navami, R. Basavaraj, S. Sharma, B. D. Prasad, and H. Nagabhushana, Journal of Alloys and Compounds **762**, 763 (2018).

[27] L. Xu, G. Li, A. Jia-Yi, J. Li-Tao, Y. Zhi-Ping, Y. Yan-Min, L. Pan-Lai, and F. Guang-Sheng, Chinese Physics Letters **28**, 027805 (2011).

[28] J. Manam and S. Das, Journal of physics and Chemistry of Solids **70**, 379 (2009).

[29] S. Katyayan and S. Agrawal, Journal of Materials Science: Materials in Electronics **31**, 8472 (2020).

[30] N. Tiwari, R. Kuraria, and S. Kuraria, Adv. Phys. Lett **1**, 15 (2014).

[31] C. Furetta, "Handbook of thermoluminescence (singapore; river edge, nj," (2003).

[32] V. Pagonis, G. Kitis, and C. Furetta, *Numerical and practical exercises in thermoluminescence* (Springer Science & Business Media, 2006).

[33] S. Katyayan and S. Agrawal, Journal of Materials Science: Materials in Electronics **28**, 18442 (2017).